Kovove Mater. 49 2011 375–383
DOI: 10.4149/km_2011_5_375

Effects of lubricant and temperature on friction coefficient during hot forging of Nimonic 115 superalloy

D. Shahriari[1]*, M. H. Sadeghi[2], G. R. Ebrahimi[3], K. T. Kim[1]

[1] *Mechanical Engineering Department, Pohang University of Science and Technology, 31 Hyoja-dong, Namgu, Pohang 790-784, South Korea*
[2] *Mechanical Engineering Department, Manufacturing Group, Faculty of Engineering, Tarbiat Modares University, Tehran, Iran*
[3] *Metallurgical and Materials Engineering Department, Ferdowsi University of Mashhad, Mashhad, Iran*

Received 2 February 2010, received in revised form 29 April 2011, accepted 10 May 2011

Abstract

In this paper, the effects of friction and temperature on Nimonic 115 superalloy are presented during hot forging. Various contact conditions were applied including dry contact and lubricated conditions using graphite, glass and mica sheets in hot ring compression and hot compression processes. The FEM simulations were carried out to derive friction factors during hot ring compression test. An upper bound method was employed to calculate friction factor during hot compression. The microstructures of samples were also examined after hot compression tests from optical microscopic observations. The partial and full dynamic recrystallization was observed at 1100 °C and 1175 °C, respectively. It was found that a mica sheet was useful for hot forging of Nimonic 115. Its friction coefficient was found by two different methods to be approximately 0.3.

K e y w o r d s: nickel base superalloy, Nimonic 115, hot compression, hot ring compression, friction coefficient, lubricant, upper bound method, dynamic recrystallization, necklace structure

1. Introduction

To improve energy efficiency and the working environment in metal forming processes, friction is considered as the key parameter to achieve this goal. Friction between the die and the workpiece plays an important role in determining the quality of the final product as well as the life of the die in metal forming processes such as forging, rolling, extrusion, drawing, and sheet metal working. As a consequence, knowledge of frictional conditions during plastic deformation is essential for the optimum design of dies. From the viewpoint of CAD/CAE, better understanding of the friction behavior can lead to more precise numerical modeling, thus permitting designers an intermediate stage of die development. In order to reduce the detrimental effects of friction, lubricants are used extensively. Hence, lubrication is critical during the forming of metals. Inadequate lubrication or a breakdown of the lubricant films can cause direct contact of the workpiece and die, and transfer of the softer workpiece material to tool surface, as well as build-up of particles on the tool, i.e. galling. Galling is a common problem that may change the tool geometry and increase the forming force. Thus, the proper selection of lubricant type reduces energy consumption, premature tool wear and consequently has an influence on production [1–8]. Ni-based superalloys are primarily used in manufacturing of critical gas turbine components such as rotating blades. The Nimonic series of superalloys possess a superior high-temperature creep resistance and oxidation resistance. In these alloys, the maximum limit of temperature for effective use increases with the complexity of the alloys and the phases present in them. On the other hand, the alloying additions and the phases present in the matrix greatly influence the hot workability of the materials [9–11]. It is evident from the above description of Nimonic superalloys

*Corresponding author: tel.: +82542792164; fax: +82542795569;
e-mail address: da_shahriari@yahoo.com, dshahriari@postech.edu

that a comparative study on the friction behavior will be useful in bringing out the influence of lubricants and temperature during hot forging. Venugopal et al. [12] compressed unlubricated ring specimens made of Armco iron and concluded that varying temperature range between 30 ℃ and 1000 ℃ did not have a significant effect on the magnitude of the shear factor m. Sadeghi and Dean [13] investigated the effect of temperature on friction using the ring compression test. The tests were carried out using steel specimens with a graphite based lubricant. It was shown that in the range of temperature 700–1150 ℃, a magnitude of the shear factor m increased with increasing temperature. Ring calibration curves are dependent upon the strain rate sensitivity as well as the ring geometry [14]. Wang and Lenard [15] studied interfacial friction on hot ring compression test in which the strain rate and temperature were identified as the significant factors affecting the frictional shear factor at the interface of the die-workpiece. At true strain rates 0.005–5 s^{-1} in the range of temperature 900–975 ℃ using a glass based lubricant, the experiments showed that the shear factor m dropped from 0.35 to 0.1 with increasing strain rate. Rudkins et al. [16] showed that for steel specimens, increasing temperature caused the level of friction to increase. Sofuoglu and Rasty [17] recommended – although the ring compression test is an effective method for determining the coefficient of friction during large deformation processes – the use of a generalized friction calibration chart regardless of the material type, and test conditions must be avoided. Lee et al. [18] investigated the influence of die velocity on the friction factor for aluminum and bronze. They showed the coefficient of friction that the friction factor decreased when the die velocity increased. Hence, there is a need to determine the friction factor and suitable lubricant for hot forging of Nimonic 115 superalloys. Friction coefficient between the dies and a workpiece by means of hot compression test (the upper-bound theory, the constant friction factor is determined by using the barrel compression test) and hot ring compression test (finite element simulation) is derived. The emphasis of this paper is on the effect of friction on variations in temperature and lubricant during hot forging of Nimonic 115 superalloy with a constant strain rate.

2. Friction modeling

2.1. Analysis of friction in Finite Element Method (FEM)

In the present work, the FEM formulation based on an updated Lagrangian description was employed to simulate the hot ring test process. To allow the focus to be placed on thermomechanical effects on the workpiece, a rigid viscoplastic material formulation coupled with a heat transfer formulation was used for the workpiece [4–8]. For problems such as ring compression, rolling and forging, the unknown direction of the relative velocity between the die-workpiece interfaces makes it difficult to handle boundary conditions in a straightforward manner. In order to deal with these situations, a velocity dependent frictional stress is used as an approximation to the condition of constant frictional stress.

2.2. Constant friction model

At the interface the velocity boundary condition is given in the direction normal to the interface by the die velocity and the traction boundary condition is expressed by:

$$\sigma_{\mathrm{t}} = -m\,k\,\frac{v_{\mathrm{S}}}{|v_{\mathrm{S}}|}, \tag{1}$$

where m is the friction factor (it varies from 0 to 1), k is the shear yield stress, and v_{S} is the sliding velocity. The negative sign characterizes the opposition between the friction stress and the velocity direction. The friction factor m is a constant including all parameters, other than the shear yield which is a suppressed constant, or without influence on the friction stress.

2.3. Coulomb friction model

The Coulomb friction model implies a linear relationship between the friction stress and the contact pressure:

$$\sigma_{\mathrm{t}} = -\mu\,\sigma_{\mathrm{n}}\,\frac{v_{\mathrm{S}}}{|v_{\mathrm{S}}|}, \tag{2}$$

where μ is the friction coefficient. Equation (1) describes the frictional conditions better than the Coulomb friction law especially at high pressure conditions in metal forming. Coulomb friction is considered to be valid only for low normal stress. Thus, the finite element discretization procedure is based on Eq. (1) in mind for the die-workpiece interface boundary condition. Using analytical methods, different sets of curves called calibration curves are obtained to determine the values of m or f for a specific lubricant. The shape of these curves is mainly influenced by the initial geometry of the ring used in the analysis. The calibration curves for m are like those shown in Fig. 1 [8].

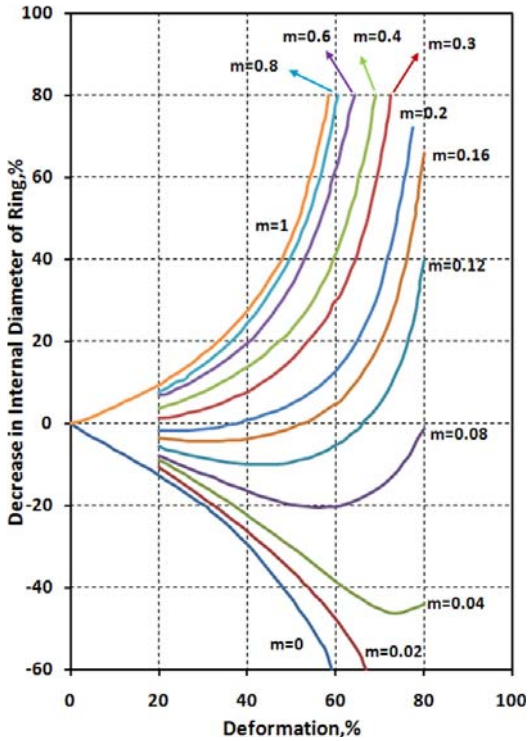

Fig. 1. Theoretical calibration curve for standard ring with an OD : ID : thickness ratio of 6 : 3 : 2 [8].

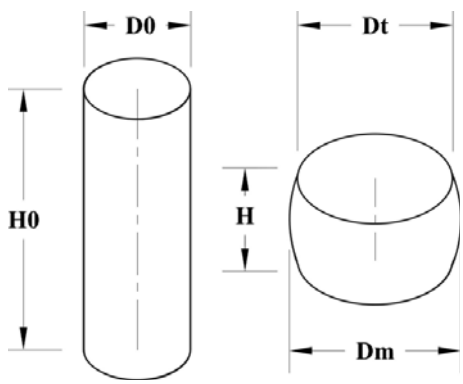

Fig. 2. Cylindrical compression test geometry.

2.4. Analysis of friction by Upper Bound Method (UBM)

The UBM theorem states that the rate of total energy associated with any kinematically admissible velocity field defines an upper bound to the actual rate of total energy required for the deformation [4–8]. For plastic deformation the external power J supplied by the platens is:

$$J = W_\mathrm{i} + W_\mathrm{f} + W_\mathrm{a} + W_\mathrm{t} = \int_\mathrm{V} \bar{\sigma}\dot{\bar{\varepsilon}}\mathrm{d}v + \int_{S_\mathrm{F}} mK\,|\Delta V_\mathrm{S}|\mathrm{d}s + \int_{S_\mathrm{D}} K\,|\Delta V_\mathrm{t}|\mathrm{d}s - \int_{S_\mathrm{T}} T_\mathrm{i} V_\mathrm{S}\mathrm{d}s. \quad (3)$$

The first term on the right hand side denotes the rate of internal energy dissipation W_i, the second term denotes the frictional shear energy losses W_f, the third term denotes the energy dissipation due to inertia forces W_a, and the last term covers power supplied by predetermined body tractions W_t. In this case, forces due to inertia are negligibly small and no external surface traction is stipulated. Therefore, $W_\mathrm{a} = W_\mathrm{t} = 0$. A simple representation of solid compression test is shown in Fig. 2. The origin of the cylindrical coordinate system is at the center of the disk. The two platens move toward each other at the same absolute velocity $\dot{U}/2$. Because of symmetry, and to facilitate computation, the upper half of the disk is considered. Now, the external power J supplied by the press is:

$$J = -\pi R^2 \dot{U} P_\mathrm{ave}\ . \quad (4)$$

The internal power of deformation is given by:

$$\dot{W}_\mathrm{i} = \frac{-\pi\sigma_0}{3\sqrt{3}}\frac{\dot{U}}{H} bR^3 \left[\left(1 + \frac{12}{R^2}\frac{H^2}{b^2}\right)^{3/2} - \left(\frac{12}{R^2}\frac{H^2}{b^2}\right)^{3/2}\right]. \quad (5)$$

The friction loss is given by:

$$\dot{W}_\mathrm{f} = -\pi m \frac{\sigma_0}{3\sqrt{3}}\frac{\dot{U}}{H}\frac{\mathrm{e}^{-b/2}}{\mathrm{e}^{-b/2}-1} bR^3. \quad (6)$$

Equating the external power with the internal power of deformation plus friction loss (Eq. 3), one obtains:

$$\frac{P_\mathrm{ave}}{\sigma_0} = 8b\frac{R}{H}\left\{\left[\frac{1}{12} + \left(\frac{H}{R}\right)^2 \frac{1}{b^2}\right]^{3/2} - \left(\frac{H}{R}\right)^3 \frac{1}{b^3} - \frac{m}{24\sqrt{3}}\frac{\mathrm{e}^{-b/2}}{\mathrm{e}^{-b/2}-1}\right\}. \quad (7)$$

To minimize P_ave, the optimum b must be chosen from

$$\frac{\partial}{\partial b}\left(\frac{P_\mathrm{ave}}{\sigma_0}\right) = 0 \quad (8)$$

after some simplifications of this equation. Thus,

$$m = \frac{(R/H)b}{(4/\sqrt{3}) - (2b/3\sqrt{3})}, \quad (9)$$

Table 1. Chemical composition of Nimonic 115 (wt.%)*

Ni	Cr	Co	Ti	Al	Mo	Fe	C	Si	Mn	Zr	Cu
bal.	14.34	13.3	3.79	4.98	3.26	0.3	0.14	0.14	0.08	0.057	0.02

*Average of at least three analyses

where

$$b = 4\frac{\Delta R}{R}\frac{H}{\Delta H} \quad (b\text{: barreling value}), \tag{10}$$

$$\Delta R = R_{\mathrm{M}} - R_{\mathrm{T}}, \tag{11}$$

$$R = R_0\sqrt{\frac{H_0}{H}}. \tag{12}$$

By measuring the top radius, the maximum radius, and the height of the cylinder after deformation (Fig. 2), by using Eqs. (9)–(12), the constant friction factor can be calculated.

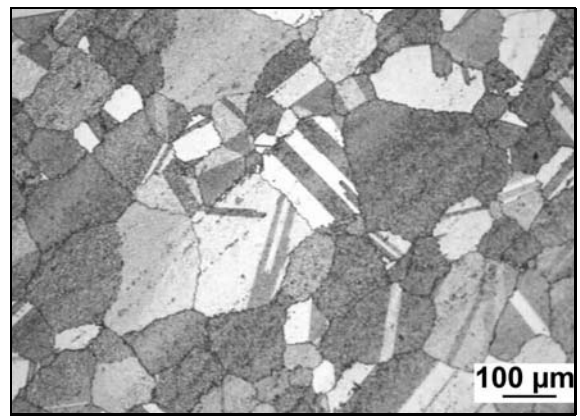

Fig. 3. Optical micrograph of the solutionized Nimonic 115.

3. Experimental procedure

In this study, hot compression test and hot ring compression test have been carried out on Nimonic 115. Its chemical composition obtained by spectrometry is given in Table 1. This material was received in the form of hot rolled bars. Cylindrical specimens were machined from the bar to have dimensions of 9 mm in height with a 1.5 height-to-diameter ratio. Rings with dimensions of 11 mm in outer diameter, 6 mm in inner diameter, and 6 mm in height were machined. Solution treatments [11] were carried out to all samples before being used in the experiments. First, the specimens were heated from room temperature to 1190 ℃; secondly, the specimens were kept constant at 1190 ℃ for 1.5 h; thirdly, the specimens were furnace cooled to 1000 ℃; finally, the specimens were air cooled to room temperature. The microstructure of the material after solution treatment is shown in Fig. 3.

A computer-controlled, servo-screw type 250 kN Zwick/Roell testing machine was used for hot compression and hot ring compression. It could be programmed to simulate both thermal and mechanical industrial process variables for a wide range of hot deformation conditions, as shown in Fig. 4. The rings were compressed isothermally between two flat polished dies to 25 %, 40 % and 55 % reductions in height using constant crosshead speeds corresponding to nominal strain rate of $1\,\mathrm{s}^{-1}$ at constant temperatures 1100 ℃ and 1175 ℃ (shown schematically in Fig. 5). In addition, four different interface lubrication conditions were used: (1) graphite powder, (2) glass powder, (3) a mica sheet and (4) unlubricated

Fig. 4. Hot compression test machine.

condition (dry). Lubricant covered the entire surface of a specimen except for a mica plate which was applied only on the active end surfaces of the specimen. This condition was considered for hot compression experiments.

To observe the evolution of microstructure during compression tests, the deformed specimens were sectioned parallel to the compression axis and prepared for metallographic examination using standard pro-

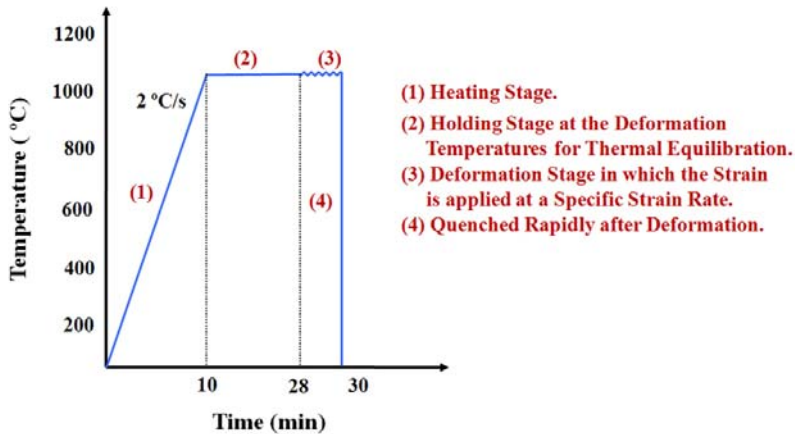

Fig. 5. The heating and deformation schedule.

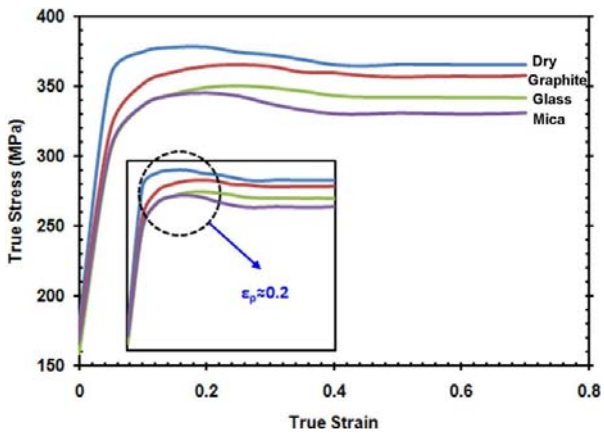

Fig. 6. True stress-strain curves Nimonic 115 at 1100 °C.

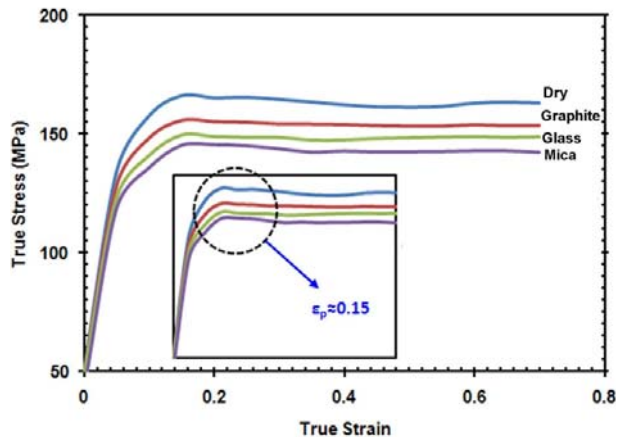

Fig. 7. True stress-strain curves Nimonic 115 at 1175 °C.

cedures and then examined by an optical microscope. The metallographic samples were etched by using a solution of $CuSO_4$ (10 g) + HCl (50 ml) + H_2O (50 ml). FEM simulations were conducted to develop calibration curves from which the operative interface friction shear factors, m, could be determined by cross plotting the data from hot ring compression. For this purpose, the FEM program DEFORM-3D was employed. The FEM simulations have been made using thermo-mechanical coupled analysis, where all material data are given as a function of temperature. Simulations using m values of 0.0 to 1.0 were performed to determine the calibration curves.

4. Results and discussion

4.1. Flow stress-strain behavior

Typical true stress-true strain curves of the Nimonic 115 in different friction conditions are presented in Figs. 6 and 7. The shapes of the true stress-true strain curves are in agreement with the usually observed deformation characteristics of nickel base superalloys [19, 20]. The flow stress at a given strain increases with decreasing temperature, thereby exhibiting typical characteristics of metals deformed in hot compression conditions.

The flow stress increases to a peak with increasing strain and then decreases as the strain further increases, which is more significant at lower temperature. The initial rapid rise in stress is associated with an increase in dislocation density resulting from work hardening. Particularly at high strain rate, the flow softening behavior or stress drop in the stress-strain curves indicates the generation of dynamic recrystallization, dynamic recovery, or cracks during hot compression. In the alloys with low or intermediate stacking fault energy, e.g. nickel or stainless steel, the dynamic recovery proceeds slowly [21]. Therefore, the dynamic recrystallization is an important cause of the decrease in flow stress.

The flow stress curves (Figs. 6 and 7) indicate such characteristics: there is an initial work harden-

ing, which leads to a pronounced peak stress; follow a steady state in the flow stress at higher strains which is then reached. This type of flow behavior approves the form of dynamic recrystallization process [22]. The peak stress increases with decreasing deformation temperature and the peak strain also increases with decreasing deformation temperature. Flow softening observed can be attributed to the adiabatic heating at strain rate $1\,s^{-1}$. The heat generated due to the plastic deformation is not conducted away since the time available is very short. Adiabatic heating effect, caused by hot deformation at this strain rate, can be encouraged by dynamic recrystallization at these temperatures, e.g. 1100 °C. Therefore, dynamic recrystallization is considered as the high temperature softening mechanism of Nimonic 115 and can be confirmed by analysis of the microstructures. Nickel base superalloys are usually considered to be low stacking fault energy materials. Therefore, dynamic recrystallization is responsible for the high temperature deformation mechanism of Nimonic 115 superalloy. Figure 8 shows the optical microstructures of samples deformed at different deformation temperatures. It is found that the fraction of recrystallized grains decreases with the increase of deformation temperature. The condition for the growth of a dynamically recrystallized grain is thought to be dependent on the distribution and density of dislocations. It can be seen that the evolution of microstructures is strongly temperature-sensitive. New recrystallized grains are seen to occur as necklace structures at 1100 °C and fully recrystallized grains at 1175 °C. It can be concluded that hot deformation at 1100 °C leads to a partially recrystallized structure and hot working processes have to be avoided below this temperature.

The necklace structure is a partially recrystallized structure consisting of a bimodal distribution of grain size, large grain size surrounded by smaller recystallized grains. In the majority of applications, the grain size requirements fall in the uniform category that happened at 1175 °C.

4.2. Lubricant consideration

The lubrication processes can take many different forms, depending on the geometry of the contacting bodies, the roughness and texture of the sliding surfaces, the contacting load, pressure and temperature, the rolling and sliding speeds, the environmental conditions, the physical and chemical properties of the lubricant, the material composition, and the properties of the near-surface layer [4, 8]. For the deformation conditions in this work, the application of mica lubricants is suggested. In this research, the results of which are given in Figs. 6 and 7 show that measured flow stress varies with the friction conditions. The highest stress-strain curve pertains to hot compression test without lubricant and other curves are related to graphite, glass and mica lubricants. It was determined that for the mica sheet, a controlled friction effect was achieved that gave the lowest flow stress values and minimized shearing and barreling of the specimens for the deformation processing conditions used in this study. The factors affecting flow stress are metallurgical structure, phase, and grain size prior deform-

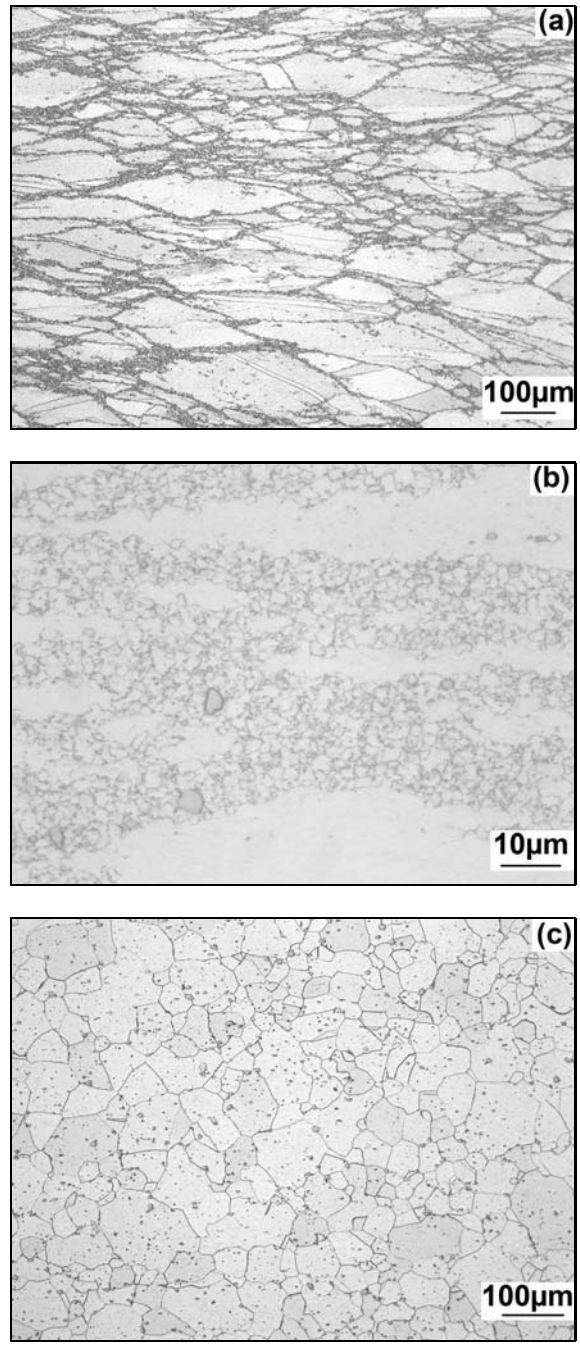

Fig. 8. Optical micrographs of Nimonic deformed with strain rate of $1\,s^{-1}$ at different temperatures of (a) 1100 °C, (b) necklace structure at 1100 °C, and at (c) 1175 °C.

Fig. 9. The plan view of the deformed Nimonic 115 rings with different lubricants.

ation, temperature of deformation, strain and strain rate, all of which have been fixed in this study. Therefore, variation of true stress is only due to different friction conditions, although with increasing friction a redundant work increases.

4.3. Friction consideration

The parameters and variables that affect the interfacial friction factor of the Nimonic 115 involve the surface condition, temperature, strain rate, the geometry of the specimen, etc. Amongst them, the effects of temperature and the geometry (ring and cylinder samples) are studied. The deformed rings for each lubricant from experiments are shown in Fig. 9. They are ordered from high to low friction. The results of FEM simulation for hot ring compression are illustrated in Figs. 10 and 11. These figures show the changes of friction coefficient with increasing reduction in height for different temperatures. In all cases, the coefficient of friction decreases with reduction in height. The values of the average coefficient of friction range from approximately 0.3 to 0.7 for mica, glass, graphite, and dry condition used in ring compression tests. The differences would have effects on loads and stresses during most industrial hot forging operations. The results from the mica sheet show that the smaller forging load is associated with lower friction. It is clear that friction is reduced by decreasing initial roughness. However, the dry condition showed the largest value of friction coefficient. This is due to the concentric grooves of a machined surface during hot ring deformation. As shown in Figs. 10 and 11, the quantity of lubricant retained may have a part to play in the friction reduction. Results suggest that the quantity of lubricants retained on the surface aided friction reduction. From experiments and simulations for hot ring compression, it is clear that the application of different lubricants at various temperatures produced different deformed profiles and surface roughness of the rings. When using lubricants with low friction coefficients such as mica and glass, an enlarged inner diameter of the specimens was obtained whilst the results were reduced of the inner diameter for lubricants with high friction coefficients such as graphite and dry condition as shown in Fig. 9. Such dimensional changes of ring specimens are also shown by the FE simulations. Therefore, the mica sheet used in hot ring compression for Nimonic 115 at elevated temperatures provides excellent lubrication. It was observed with an increase in temperature, the

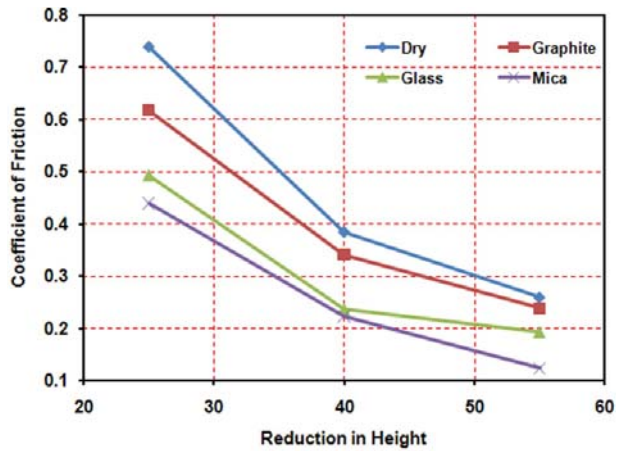

Fig. 10. Variations of friction coefficients during hot ring compression test at 1100 °C.

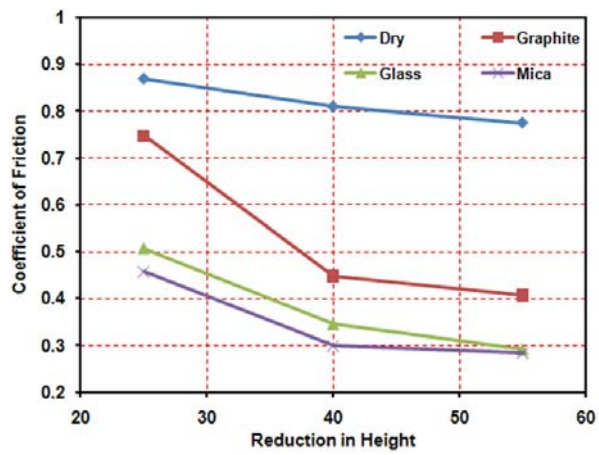

Fig. 11. Variation of friction coefficients during hot ring compression test at 1175 °C.

friction coefficient m increases to full sticking.

In Fig. 12, a temperature versus friction factor for hot ring compression is shown. The present investigation also shows temperature variations have little effect on the friction factor of mica lubricant. It seems the average of friction coefficients remain nearly constant on mica lubricant during an increase of temperature. In order to compare hot ring compression method with analytic method which has been described in this study, hot compressions were carried out on Nimonic 115 by using previous lubricants. Figure 13 shows sample cylinders after deformation with

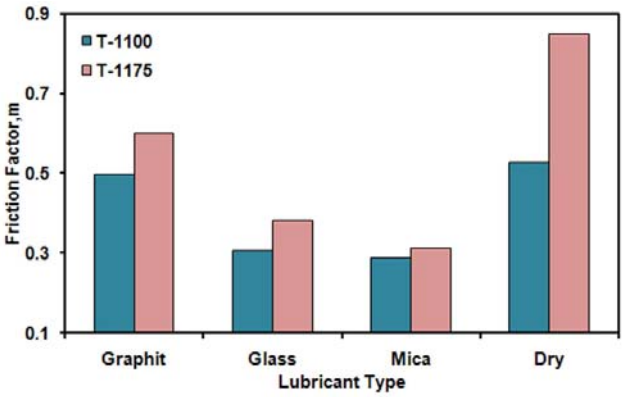

Fig. 12. Dependence of the friction factor on temperature using different lubricants during hot ring compression test.

Table 2. Friction factors estimated during hot deformation

Lubricant type	Test method	Measured average friction factor
Mica	Hot ring compression	0.301
	Hot compression	0.284
Glass	Hot ring compression	0.344
	Hot compression	0.297
Graphite	Hot ring compression	0.55
	Hot compression	0.441
Dry	Hot ring compression	0.689
	Hot compression	0.458

different degrees of barreling. The degree of barreling of cylinders after deformation depends on the friction condition. Barreling occurs due to friction between the workpiece and the die, so the application of a suitable lubricant may reduce friction but will never eliminate it completely. During each experiment, the maximum and top radius of cylinders (R_M, R_T) and height of cylinders after deformation were measured.

The constant friction factor m at 1100 ℃ and 1175 ℃ was calculated by Eq. (9). The results, a compilation of which is calculated for hot compression test, are plotted in Fig. 14. Figure 14 shows that the mica sheet has friction coefficients of $m = 0.269$ and 0.297 at 1100 ℃ and 1175 ℃, respectively. Thus, mica used in hot compression for Nimonic 115 at elevated temperatures provides an excellent lubrication and behaves similarly in hot ring compression. It can be observed that the shear strength of the glass and mica lubricants is directly proportional to viscosity. Therefore with the decrease in viscosity of glass and mica lubricants, their shear strength and friction factors are reduced. At high temperatures, the mica lubricant possesses liquid characteristics. At strain rate of $1\,s^{-1}$, there is no sufficient time for the lubricant to be squeezed out, resulting in favorable lubrication conditions and low values of m, as shown in Figs. 12 and 14.

Investigations on deformation of rings and cylinders with various lubrication conditions are summarized in Table 2. The average friction factors at 1100 ℃ and 1175 ℃ are shown. Comparison of these results shows the effect of geometry and optimum barreling on friction factor during hot compression and hot ring compression. It is noteworthy to mention that hot ring compression is a very useful experimental method for measuring the friction condition. The flow stress behavior of Nimonic 115 during the hot ring compression has not a great importance for designer of hot forging processes. Thus, when the hot compression test is performed, it is possible to predict the flow stress, friction behavior, friction coefficient and microstructural evolutions of this material.

The results of hot compression for calculation of friction factor using obtained data can be reasonable in predicting actual results during hot forging process.

5. Conclusions

Based on the studies presented in this paper, the following conclusions are drawn:

– Hot compression test is a useful method to estimate the flow stress behavior and performance of a lubricant.

– Flow stress curves indicate that the optimum hot ductility of Nimonic 115 is observed at 1175 ℃ and the strain rate $\dot{\varepsilon} = 1\,s^{-1}$.

– The partial and full dynamic recrystallization is observed at 1100 ℃ and 1175 ℃, respectively.

– The major advantage of using hot compression for driving of the friction factor is dependent only on the geometrical measurement of the shape change.

Fig. 13. The plan view of the deformed Nimonic 115 cylinders with different lubricants.

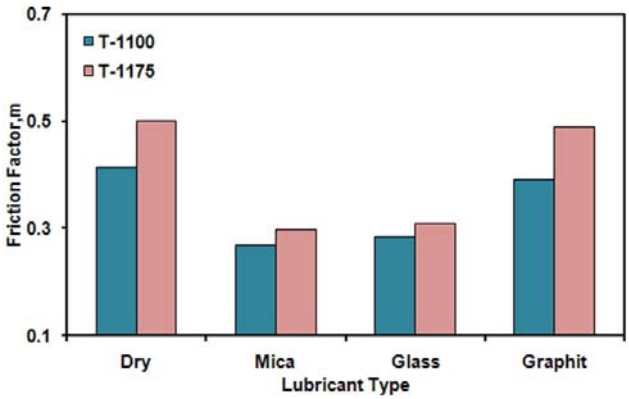

Fig. 14. Dependence of the friction factor on temperature using various lubricants during hot compression.

– A mica sheet is an excellent lubricant for hot forging of Nimonic 115. The friction coefficient remains nearly constant at different high temperatures and its value is approximately 0.3.

– The value of friction factor for lubricants other than mica increases with the increase in temperature.

Acknowledgements

The authors wish to sincerely thank Prof. M. J. Nategh, Prof. A. Akbarzadeh, Prof. M. Jahazi, Engineers A. Amiri and M. Cheraghzadeh for their valuable discussions in this research.

References

[1] BAKHSHI-JOOYBARI, M.: J. Mater. Process. Technol., *125/126*, 2002, p. 369. doi:10.1016/S0924-0136(02)00343-6
[2] HAYHURST, D. R.—CHAN, M. W.: Int. J. Mech. Sci., *47*, 2005, p. 1. doi:10.1016/j.ijmecsci.2004.12.008
[3] SOFUOGLU, H.—GEDIKLI, H.: Tribol. Int., *35*, 2002, p. 27.
[4] ALTAN, T.—NGAILE, G.—SHEN, G.: Cold and Hot Forging. Ohio, USA, ASM International 2004.
[5] STUZALEC, A.: Theory of Metal Forming Plasticity Classical and Advanced Topics. Berlin, Springer 2004.
[6] KOBAYASHI, S.—OH, S. I.—ALTAN, T.: Metal Forming and the Finite Element Method. New York-Oxford, Oxford University Press 1989.
[7] WAGONER, R. H.—CHENOT, J. L.: Fundamental of Metal Forming. New York, John Wiley & Sons 1996.
[8] DIETER, G. E.—KUHN, H. A.—SEMIATIN, L.: Handbook of Workability and Process Design. Ohio, USA, ASM International 2003.
[9] DONACHIE, M. J.—DONACHIE, S. J.: Superalloys a Technical Guide. Ohio, USA, ASM International 2002.
[10] PARK, N. K.—KIM, I. S.—NA, Y. S.: J. Mater. Proc. Technol., *111*, 2001, p. 98. doi:10.1016/S0924-0136(01)00489-7
[11] SHAHRIARI, D.—SADEGHI, M. H.—AKBARZADEH, A.: Mater. Manuf. Process., *24*, 2009, p. 559.
[12] VENUGOPAL, S.—SRINIVASAN, G.—VENKADESAN, S.—SEETHARAMAN, V.: J. Mech. Work. Technol., *19*, 1989, p. 261.
[13] SADEGHI, M. H.—DEAN, T. A.: Int. J. Mach. Tool. Manu., *30*, 1990, p. 509. doi:10.1016/0890-6955(90)90003-2
[14] GOETZ, R. L.—JAIN, V. K.—MORGAN, J. T.—WIERSCHKE, M. W.: Wear., *143*, 1991, p. 71. doi:10.1016/0043-1648(91)90086-A
[15] WANG, F.—LENARD, J. G.: J. Eng. Mat. Technol., *114*, 1992, p. 13.
[16] RUDKINS, N. T.—HARTLEY, P.—PILLINGER, I.—PETTY, D.: J. Mater. Proc. Technol., *60*, 1996, p. 349. doi:10.1016/0924-0136(96)02353-9
[17] SOFUOGLU, H.—RASTY, J.: Tribol. Int., *32*, 1999, p. 327.
[18] LEE, C. D.—WENG, C. I.—CHANG, J. G.: Metall. Trans. B, *32 B*, 2001, p. 137.
[19] MASHREGHI, A. R.—MONAJATIZADEH, H.—JAHAZI, M.—YUE, S.: Mater. Sci. Technol., *20*, 2004, p. 161. doi:10.1179/026708304225010343
[20] BRAND, A. J.—KARHAUSEN, K.—KOPP, R.: Mater. Sci. Technol., *12*, 1996, p. 963.
[21] ZHOU, L. X.—BAKER, T. N.: Mater. Sci. Eng. A, *177*, 1994, p. 1. doi:10.1016/0921-5093(94)90472-3
[22] SAKAI, T.—JONAS, J. J.: Acta Metall., *32*, 1984, p. 189.